Magnetic Behavior of Plain Carbon Steels as A Function of Applied Stress and Strain Conditions

Edward S. GORKUNOV, Sergei V. SMIRNOV, Sergei M. ZADVORKIN, Sophia Yu. MITROPOLSKAYA, Dmitrii I. VICHUZHANIN, Institute of Engineering Science, Urals Branch of the Russian Academy of Sciences, Ekaterinburg, Russia

Abstract. A technique for restoring stress-strain diagrams of steel products by magnetic characteristics determined directly during tension is proposed. Coercive force, the value of residual induction on the major magnetic hysteresis loop and maximum magnetic permeability are recommended as parameters of nondestructive testing of stresses and strains.

Introduction

The potentialities of nondestructive testing of the stress-strain state of ferromagnetic materials remain to be realized in full measure, though the stress and strain dependences of magnetic properties were noted by E. Villary [1] as early as in the 19th century. Numerous investigations have since been aimed at studying the effect of elastic and plastic deformations on the initial magnetization curve and the hysteresis loop [2–11]. At different times, a large number of attempts were made, with different success, to accomplish the mathematical simulation of magnetic properties as a function of stresses and strains [12–15]; however, the matter of predicting and inspecting the stress-strain state of structural members by measuring their magnetic characteristics remains a challenge.

One of the methodological difficulties is that the effect of stresses and strains on magnetic characteristics were studied under unloading, after external stresses have been relieved. There are currently not many works describing the “in situ” measurement of magnetic characteristics during deformation [16, 17].

No works describing the behaviour of the coercive force on the sharp yield point portion and the yield plateau have come to our notice. The study of magnetic characteristics at the stages prior to fracture can also be found in the literature only fragmentarily. Therefore this paper is aimed, firstly, at analyzing the behaviour of the magnetic characteristics of steels as dependent on stresses and strains under tension over the whole length of the stress-strain curve, including its least studied portions, and, secondly, at studying the possibility of using magnetic parameters for testing admissible strains in steel products and structural members.

The paper adduces some results of magnetic measurements made on low- and medium-carbon steels directly under stresses, with the simultaneous recording of stresses and strains on all the portions of the stress-strain diagram up to test piece failure.

1. Research Procedure and Material

Magnetic properties of flat specimens made of steel St3sp after annealing (800°C, 2 hours,

furnace cooling), steel 45 after normalizing (as-delivered), steel 45 after quenching (850°C, oil) with tempering (350°C, 2 hours) were studied in the course of uniaxial tension. The chemical composition of the steel grades under study is presented in table 1, the mechanical properties and structure characteristics being given in table 2.

Table 1. Fraction of total mass, %

Steel	C	Mn	Cr	Fe
St3sp	0.14–0.22	0.40–0.65	–	Balance
45	0.42–0.50	0.50–0.80	0.25	Balance

Table 2. Mechanical properties and structure

Material	Mechanical properties			Structure characteristic
	$\sigma_{0.2}$, MPa	σ_u, MPa	δ, %	
St3sp (annealing)	260	360	27	Ferrite
45 (normalizing)	360	520	14.5	ferrite+pearlite
45 (quench.+temp.)	980	1070	3.1	troosto-martensite

The mechanical properties presented in table 2 were calculated by the following formulae:

- conventional yield strength $\sigma_{0.2} = \frac{P_{0.2}}{F_0}$,

where $P_{0.2}$ is the load corresponding to the conventional yield strength; F_0 is the initial specimen cross section area;

- ultimate strength $\sigma_u = \frac{P_{MAX}}{F_0}$,

where P_{MAX} is the greatest load prior to fracture;

- specific elongation after rupture $\delta = \frac{(l_k - l_0)\cdot 100}{l_0}$,

where l_k is the final gauge length; l_0 is the initial gauge length.

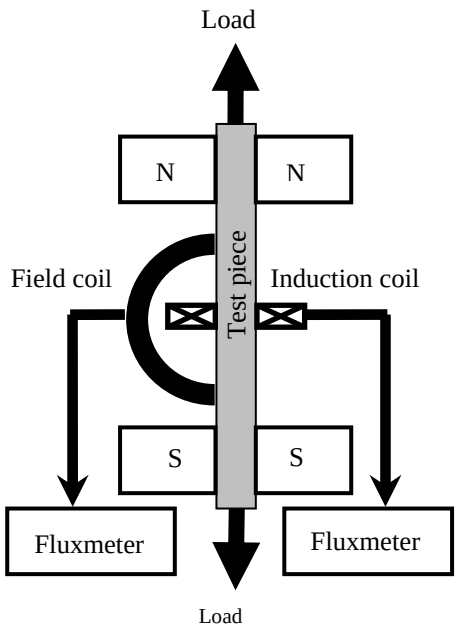

Fig. 1. Test scheme

The experiment was conducted on the facility schematically shown in fig. 1. The measurements of internal fields under magnetization reversal were made by a permeameter circuit on an installation comprising a standard computerized hysteresisgraph. Magnetic field was applied along the tension axis, the axis of the search induction coil being parallel with the tension axis too. The internal magnetic field strength H was measured by a magnetic potentialmeter. The magnetic hysteresis loop at the maximal internal field kA/m to -60 kA/m (the figures show only those segments of H_{max}=60 kA/m was recorded on the B-H plane by memorizing 2500 points. The field and induction measurement error did not overshoot ±3 %. Hysteresis loops and resulting magnetic parameters were examined. The field dependence of differential magnetic permeability was obtained by differentiating the falling branches of the corresponding major magnetic hysteresis loops with respect to the field in the range from +60 the field dependences that have permeability peaks).

Tension was performed at room temperature. The test pieces had a gauge length of 90 mm,

width of 20 mm and thickness of 1 to 2 mm for different steels. The tests were run on an experimental machine with a maximum force of 50 kN, with an active grip moving at 2 mm/min. Strain under stressing was evaluated by raster displacement pickups affixed directly to the specimen. The tests were conducted with a notably small elongation step over the whole interval of the stress-strain diagram up to specimen fracture. At each step, when a certain degree of strain was attained, stressing was suspended without relieving, and magnetic hysteresis loops were measured. Tension was resumed thereafter up to the next measurement point. The specimen was demagnetized before and after each magnetic measurement.

The true strain ε_i on the *i*-th step of stressing to necking was determined by the formula for plane flow conditions

$$\varepsilon_i = ln(l_i/l_0) \quad (1)$$

where l_0 is the initial gauge length and l_i is the gauge length after the *i*-th stressing.

After necking, ε was determined by the formula found in [18] as

$$\varepsilon_i = \frac{2}{\sqrt{3}} \cdot \sqrt{\left(\ln\frac{b_i}{b_0}\right)^2 + \ln\frac{b_i}{b_0} \cdot \ln\frac{h_i}{h_0} + \left(\ln\frac{h_i}{h_0}\right)^2} \quad (2)$$

where $b_0, h_0,$ and b_i, h_i are the specimen cross section area before and after the deformation.

The true stress σ_i on the *i*-th step of stressing was determined by the formula

$$\sigma_i = F_i/S_i \quad (3)$$

where P_i is the load applied to the specimen at the *i*-th stressing, F_i is the specimen cross section area at the *i*-th stressing, which was determined at the stage of uniform deformation from the condition of the constancy of the gauge part volume as

$$F_i = F_0 \cdot l_0/l_i \quad (4)$$

where F_0 is the initial cross section area of the gauging part of the specimen. After necking, F_i was determined from the instrumental measurements.

Fracture occurred in all the test pieces near the centre of the gauge length, the gauge part immediately adjacent to the fracture zone therewith found itself in the search coil.

2. Results and Discussion

Figure 2 presents stress-strain diagrams obtained in tension to fracture.

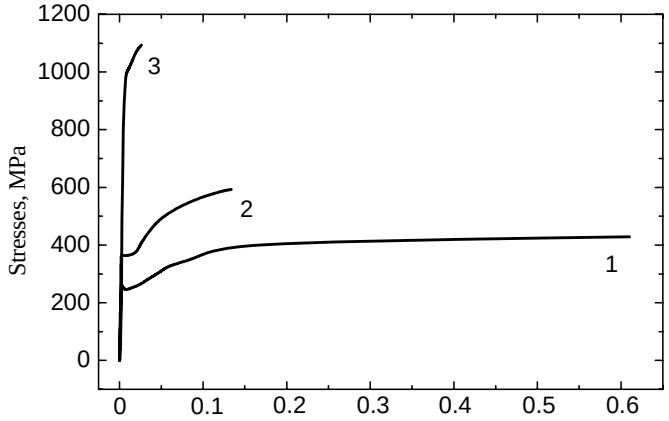

Fig. 2. Stress-strain curves for steel St3sp (1), normalized steel 45 (2) and steel 45 after quenching with tempering (3)

The diagrams and the data given in table 2 attest that steel St3sp, which deforms with a sharp yield point, is the most plastic of the three materials. Normalized steel 45 has a yield plateau at stresses of about 400 MPa, and in the plastic region it undergoes some strain

hardening. Hardened steel 45 exhibits the highest strength, but the smallest plasticity margin; the elastic-to-plastic strain transition takes place at about 1000 MPa, and the material fractures without necking shortly thereafter.

Figures 3 to 5 show the coercive force H_c, the maximal magnetic permeability μ_{max} and residual induction B_r as dependent on the degree of strain to necking for steel St3sp, for normalized steel 45 and for steel 45 after quenching with tempering respectively. The strain degree dependences of the coercive force are seen to be qualitatively similar to the stress-strain diagrams, whereas the dependences of the maximal magnetic permeability and residual induction display inverse behaviour.

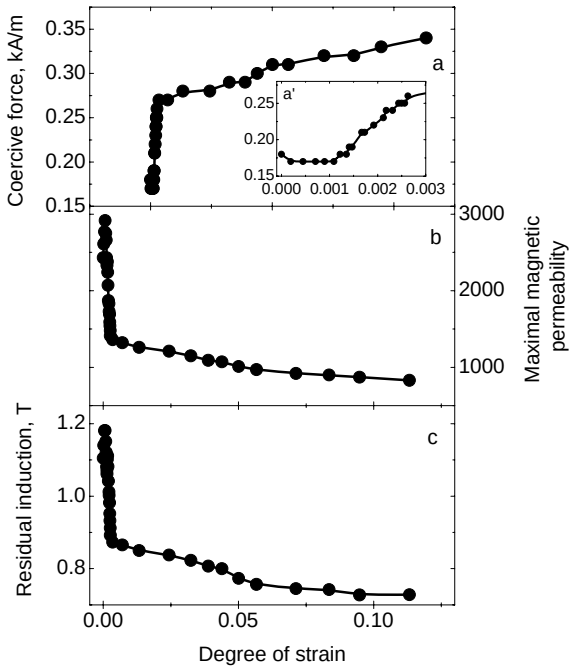

Fig. 3. Magnetic characteristics of annealed steel St3sp as functions of the degree of tensile strain (prior to necking): coercive force H_c (a), maximal magnetic permeability (b) residual induction B_r (c). The inset (a') shows the initial portions of the curve $H_c(\varepsilon)$

In order to analyse the behaviour of the coercive force under tension, the strain degree dependences of H_c with normalized values were superimposed on the corresponding stress-strain diagrams (prior to necking), see fig. 6. The normalized values of the measured characteristics were determined by the formulae $\sigma=\sigma_i/\sigma^*$ and $H_c=H_{ci}/H_c^*$, where σ^* and H_c^* correspond to the true stresses and the coercive force at the stressing P_{MAX}.

The behaviour of the coercive force has three distinct characteristic portions, namely, 1) the elastic strain region; 2) the yield plateau and/or sharp yield point; 3) the region of developed plastic strain. On the initial portion of the tensile test diagram the coercive force of the specimens made of steel St3sp and normalized steel 45 decreases by 6 and 16% respectively. At stresses exceeding 80 MPa for steel St3sp, 280 MPa for normalized steel 45 and 400 MPa for steel 45 after quenching with tempering, the dependence $H_c(\varepsilon)$ becomes practically inversely proportional up to the flow stress. In the stress range from the upper yield point to the lower one, i.e. on the portion corresponding to the sharp yield point and/or yield plateau, the coercive force stops growing to resume growing after this portion.

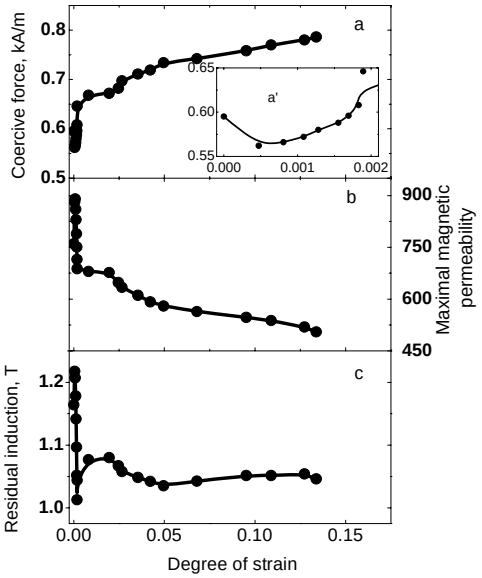

Fig. 4. The same for normalized steel 45

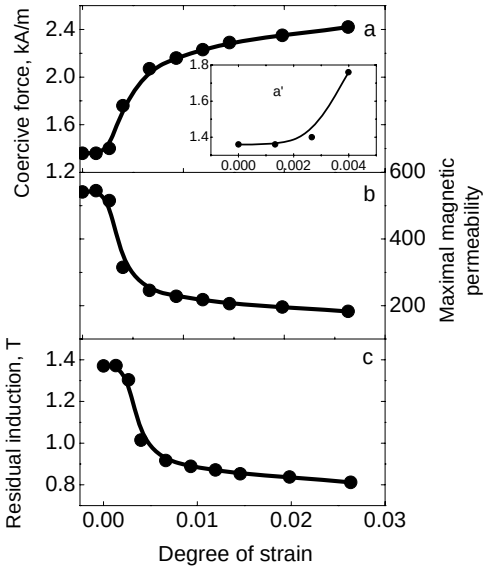

Fig. 5. The same for steel 45 after quenching with tempering

The experimentally obtained nonmonotonic dependence $H_c(\varepsilon)$ in the region of elastic stresses can be viewed as resulting from a number of effects. Thus, specimen tension in the elastic region leads to the formation of the magnetic stress texture referred to as induced magnetic anisotropy [2]. With the positive magnetoelastic effect (magnetostriction and external stresses having the same sign), the magnetic moments orient themselves along the tension axis, the coercive force decreases and magnetic permeability grows when magnetization has the same direction as tension. However, on further stressing, the magnetostriction of iron may change sign [19, 20] thus causing a negative magnetoelastic effect and changing the type of the magnetic texture. Besides, the "sign" of the magnetoelastic effect can be governed by the second magnetostriction constant λ_{111}, which is negative in iron and iron-carbon alloy crystallites. Affected by these factors, the coercive force is bound to grow.

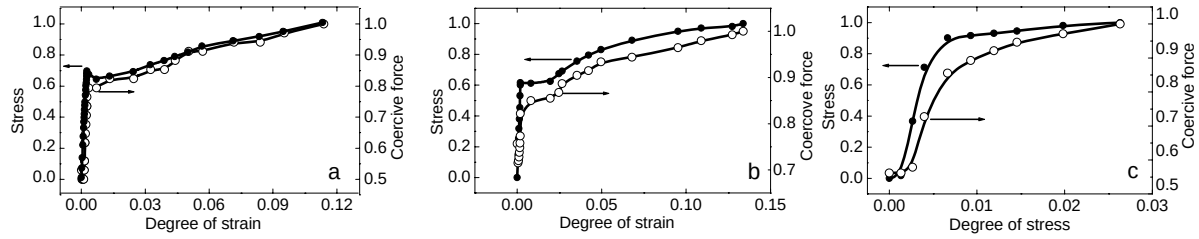

Fig. 6. Stress-strain curves (prior to necking) and superposed strain dependences of the coercive force H_c for steel St3sp (a), normalized steel 45 (b) and steel 45 after quenching with tempering (c) in normalized values.

The effect of stresses reaching and exceeding $\sigma_{0.2}$ causes the failure of the magnetic stress texture [2], and it is the growth of dislocation density ($H_c \sim N^{1/2}$ where N is dislocation density [21]) and the formation of the deformation texture that are the decisive factors affecting the coercive force in the region of plastic strain.

The peculiarities of the changes in the magnetic characteristics near and on the portion of the sharp yield point and the yield plateau invite a more detailed examination. As $\sigma_{0.2}$ is approached, the coercive force of all the specimens tested grows significantly, the most active growth of H_c being observed prior to the stress $\sigma_{0.2}$, not at $\sigma_{0.2}$, and this is consistent with

the results found in [16]. In steel St3sp the growth of the coercive force pauses upon reaching the upper yield stress, the value of H_c remains constant or slightly decreases, and then, after passing the lower yield point, it resumes growing, though less actively, see fig. 3. The sharp yield point on the tensile test diagram is known [22] to be caused by the separation of dislocations from the Cottrell atmospheres upon reaching the critical stress. The dislocation density does not increase in this case; moreover, it may sometimes decrease, as some dislocations crop out and form Chernov-Luders bands.

In the tension of normalized steel 45, which deforms with the formation of a yield plateau, the coercive force grows significantly as the stress $\sigma_{0.2}$ is approached as well, the values of H_c being stable thereafter up to the end of the yield plateau, see fig. 4. In the tension of quenched steel 45 there are no sharp yield point and yield plateau (fig. 5), the transition from elastic to plastic deformation being associated in this case with a sharp decrease in the slope of the curve $H_c(\varepsilon)$. At stresses overshooting the yield stress of the material, the decrease in the slope of the curve $H_c(\varepsilon)$ was noted on all the specimens tested, with the coercive force growing monotonically on the entire portion of plastic deformation up to specimen fracture.

It is obvious from figs 3 to 5 that the curves representing strain dependences of maximum magnetic permeability μ_{max} and residual induction B_r on the major loop are the specular reflection of the stress-strain diagram, which can thus be restored nit only by the coercive force values, but also by the function inverse to $\mu_{max}(\varepsilon)$ or $B_r(\varepsilon)$.

Figure 7 shows the coercive force measured in tension as a function of applied stresses. It is obvious from the curves that the stress dependences of the coercive force for steel St3sp and normalized steel 45 signify the onset of plastic flow very definitely, and they can be used in estimating yield stress $\sigma_{0.2}$ by the magnetic method, without strain gauging.

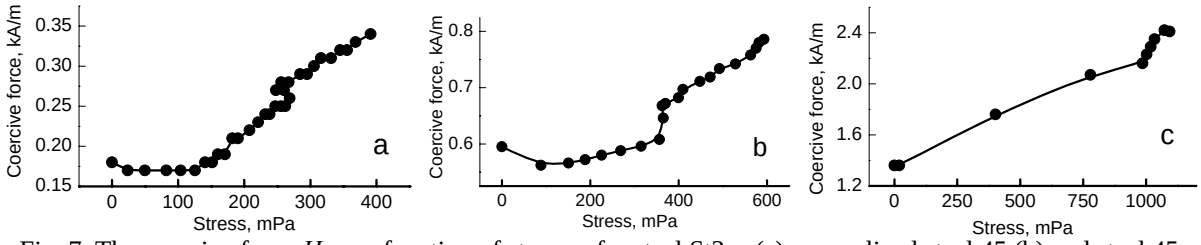

Fig. 7. The coercive force H_c as a function of stresses for steel St3sp (a), normalized steel 45 (b) and steel 45 after quenching with tempering (c)

3. Conclusion

The strain dependences of the coercive force in the tension of low- and medium-carbon steels are qualitatively similar to the stress-strain diagram up to necking, with a definitive direct relationship between $H_c(\varepsilon)$ and $\sigma(\varepsilon)$, and an inverse relationship of $B_r(\varepsilon)$ and μ_{max} to $\sigma(\varepsilon)$. The stress-strain diagrams for flat specimens made of low- and medium-carbon steels under plastic deformation in uniaxial tension can be are reproduced by the measurements of the coercive force and/or residual induction, and this enables changes in the stress-strain state of an object to be estimated.

The work was supported by the RFBR (grant 04-01-96110).

References

[1] Villary, E. Ann. Phys. Chem., **126**, 1865, p. 87.
[2] Vonsovsky, S.V., Shur, Ya.S. Ferromagnetism. – Moscow-Leningrad: OGIZ, 1948, 816p.

[3] Bozorth, R.M. Ferromagnetism. – Van Nostrand, New York, 1951, pp. 600-609.
[4] Babich, V.K., Pirogov, V.A. Physics of Metals and Metallography (Fizika metallov i metallovedenie), **28** (1969), No 3, pp. 447-453.
[5] Atherton, D.L., Jiles, D.C. NDT International, **19** (1986), pp. 15-19.
[6] Jiles, D.C. J. Phys. D: Appl. Phys., **21** (1988), pp. 1196-1204.
[7] Thompson, S.M., Tanner, B.K. J. Magn. Magn. Mater. **132** (1994), pp. 71-88.
[8] Bulte, D.P., Langman, R. A. J. Magn. Magn. Mater., **251** (2002), No 2, pp. 229-243.
[9] Langman, R. IEEE Trans. Magn., **26** (1990), pp. 1246-1251.
[10] Sablik, M.J., Kwun, H., Burkhardt, G.L. J. Magn. Magn. Mater. **140-144** (1995), pp. 1871-1872.
[11] Jayakumar, T., Vaidyanathan, S., Raj, B., Moorthy, V., Kashyap, B.P. Acta Materialia, **47** (1999), pp. 1869-1878.
[12] Sablik, M.J. Nondestr. Test. Eval., **5** (1989), pp. 49-65.
[13] Jiles, D.C., Devine, M. K. J. Magn. Magn. Mater. **140-144** (1995), pp. 1881-1882.
[14] Sablik, M.J., Jiles, D.C. Journal of Physics D: Applied Physics, **32** (1999), 1971-1983.
[15] Sablik, M.J., Yonamine, T., Landgraf, F. IEEE Trans. Magn., **40** (2004), pp. 3219-3226.
[16] Makar, J.M., Tanner, B.K. J. Magn. Magn. Mater. **184** (1998), pp. 193-208.
[17] Makar, J.M., Tanner, B.K. J. Magn. Magn. Mater. **187** (1998), pp. 353-365.
[18] Bogatov, A.A., Mizhiritsky, O.I., Smirnov, S.V. Plasticity margin of metals under plastic metal forming. – Moscow: Metallurgiya, 1984, 144 p.
[19] Dunayev, F.N. Russian Physics Journal (Izvestiya vuzov. Fizika), 1962, No 1, pp. 151–153.
[20] Zaikova, V.A., Shur, Ya.S. Physics of Metals and Metallography (Fizika metallov i metallovedenie), **21** (1966), pp. 664 – 673.
[21] Mikheyev, M.N., Gorkunov, E.S. Magnetic methods of structural analysis and nondestructive testing. – Moscow: Nauka, 1993, 252 p.
[22] Cottrell, A.H. Dislocations and plastic flow in crystals. – Moscow: State Scientific and Technical Publishing House for Ferrous and Nonferrous metallurgy, 1958, 268 p.